JFM RAPIDS
journals.cambridge.org/rapids

Unravelling the Rayleigh–Taylor instability by stabilization

A. Poehlmann, R. Richter† and I. Rehberg

Experimentalphysik V, Universität Bayreuth, D-95440 Bayreuth, Germany

A recently proposed stabilization mechanism for the Rayleigh–Taylor instability, using magnetic fluids and azimuthally rotating magnetic fields, is experimentally investigated in a cylindrical geometry and compared with the theoretical model. This approach allows the imperfection of the experimental setup to be exploited for measuring the critical field strength of the instability without ever reaching the supercritical state. Furthermore, we use a fast increase in the magnetic field strength to prevent an already occurring instability and force the system back to its initial state. In this way we measure the growth dynamics repeatedly and acquire the characteristic time scale τ_0 of the instability.

Key words: colloids, flow control, instability control

1. Introduction

The Rayleigh–Taylor instability (RTI) occurs when a dense fluid is accelerated into a less dense fluid (Rayleigh 1883; Taylor 1950). It can influence processes at all scales, from inertial confinement fusion (Evans, Bennett & Pert 1982), up to supernovae (Smarr *et al.* 1981). As the RTI is caused by gravitational acceleration and is a backward bifurcating instability without supercritical equilibrium states, it is experimentally challenging to prepare and measure. Experimental approaches comprise the sudden destruction of a diaphragm of shellac (Lewis 1950, preparation), the upside-down rotation (Völtz, Pesch & Rehberg 2001, preparation) or vertical vibration (Wolf 1969, stabilization) of the whole setup. Rannacher & Engel (2007) proposed a potentially less disturbing mechanism to stabilize high-wavenumber modes of the RTI, which uses magnetic fluids and azimuthally rotating magnetic fields.

In this article, we prove the feasibility of that stabilization mechanism. We further show that the instability can be described by a subcritical pitchfork bifurcation, and exploit the imperfection of our experimental setup to acquire the critical field strength of the RTI without ever reaching the supercritical state. The experimental results are

† Email addresses for correspondence: andreas.poehlmann@imp.ac.at, reinhard.richter@uni-bayreuth.de, ingo.rehberg@uni-bayreuth.de
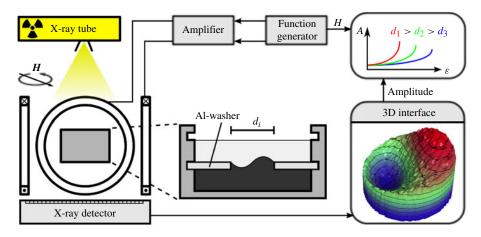
FIGURE 1. A sketch of the experimental setup with an example of a three-dimensional reconstruction of the common fluid interface. The cylindrical container is filled with both fluids and placed inside two pairs of coils, which generate an azimuthally rotating magnetic field. The size of the interface can be changed by replacing the thin aluminium washer in the experiment container. A vertically mounted X-ray setup is used to record the interface shape, while varying the strength of the magnetic field.

quantitatively compared with the stability boundary predicted by the theoretical model. The method has the advantage that a Rayleigh–Taylor unstable system can be forced back to a stable state by increasing the magnetic field, therefore recovering the initial condition and allowing repeated measurements of the dynamics of the instability. We use this procedure to measure the characteristic time scale τ_0 of the first unstable mode.

2. Experimental setup

Figure 1 shows a sketch of the experimental setup. A commercially available magnetic fluid (Ferrotec Corp., type APG512a, density $\rho_0 = 1240$ kg m^{-3}, initial susceptibility $\chi_0 = 1.4$, dynamic viscosity $\eta_0 = 75$ mPa s, surface tension $\sigma_0 = 23.8$ mN m^{-1}) and a non-magnetic fluid (Solvay Solexis Inc., Galden-SVP, $\rho_1 = 1706$ kg m^{-3}, $\eta_1 = 1.4$ mPa s, $\sigma_1 = 16$ mN m^{-1}) are used to prepare the experiment. The interfacial tension has been measured utilizing a ring tensiometer (Lauda Co., TD 1). Using the density correction by Zuidema & Waters (1941) we get $\sigma = 6.6 \pm 0.3$ mN m^{-1}. This value was corroborated by measurements with a drop volume tensiometer utilizing a drop rate of $1/60$ s (Lauda Co., TVT 2). Both fluids are poured into a cylindrical container (diameter 38 mm, depth for each fluid 5 mm), which is equilibrated with a spirit level, excluding inclinations larger than 3×10^{-4} rad. The size of their common interface can be changed by mounting thin aluminium washers with centric holes of different size. The rotating magnetic field is provided by two orthogonally oriented pairs of coils, driven by amplifiers (HKAudio, type VC2400). A function generator produces the 90° phase-shifted two-channel sinusoidal input signal for this setup. The shape of the common interface between the two fluids is measured with a vertically mounted X-ray-transmission setup (Richter & Bläsing 2001; Gollwitzer *et al.* 2007), which exploits the different attenuation coefficients of the two liquids to reconstruct the shape of the common interface.
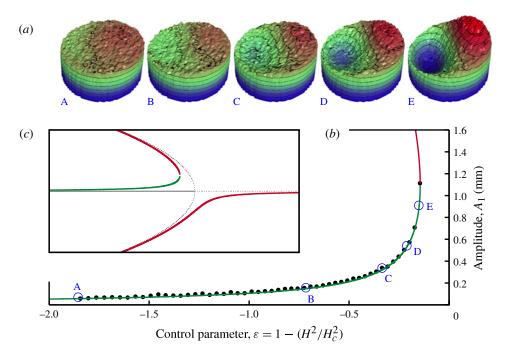
FIGURE 2. (*a*) Three-dimensional representation of the stable interface (15 mm diameter, *z* direction scaled by 10) for five different values, A–E, of the control parameter. (*b*) Control parameter dependence of the pattern amplitude, displaying every fourth data point. The fit by the stable (unstable) solution of (3.6) is marked by green (red) solid lines. (*c*) Imperfect subcritical pitchfork bifurcation in red and green. For comparison the solid (dotted) black lines denote the stable (unstable) branch of the perfect bifurcation.

The preparation of the starting condition is a two-step process. First the container is filled with the less dense magnetic fluid up to the aluminium washer. After that, the rotating magnetic field is activated at maximum field strength and the non-magnetic fluid is poured in the container, resulting in a magnetically stabilized layering of the two fluids. The amplitude of the magnetic field is then quasi-statically reduced until the system becomes unstable, while the shape of the common interface is recorded with the X-ray setup.

3. Experimental results

In the following we first present radioscopic measurements of the shape of the interface and match them with an analytical description. Second, we compare the control parameter dependence of the pattern amplitude with the scaling predicted by an imperfect amplitude equation. Third, the experimentally determined boundary of stability of the interface is compared with the model by Rannacher & Engel (2007). Finally we record the growth dynamics of the unstable interface and fit the dynamic amplitude equation.

3.1. *The shape of the interface*

Figure 2(*a*) shows five representative reconstructions of the interface at different subcritical magnetic field strengths. With decreasing field strength the circular interface

develops a prominent crest (red) and a trough (blue). The analytical function for the interface shape in an infinite domain allows us to explain the observed mode within the experimental measurement errors in the described finite geometry. Forcing terms related to the boundary conditions will therefore be absent from this equation. To obtain it, we use the equation for the magnetic potential at the common interface under the influence of an azimuthally rotating magnetic field (Rannacher & Engel 2007). Inserting this into the ferrohydrodynamic Bernoulli equation (Rosensweig 1985, §5) and linearizing the resulting differential equation for the interface yields

$$\left[-\frac{\mu_0 \chi^2 H_0^2}{(2+\chi)k} \left(\cos^2 \Omega t \partial_{xx} + \sin^2 \Omega t \partial_{yy} + \sin 2\Omega t \partial_{xy} \right) \right.$$
$$\left. - \sigma (\partial_{xx} + \partial_{yy}) + (\rho_0 - \rho_1)g \right] \times h(x,y) = 0, \tag{3.1}$$

with the permeability of free space μ_0, the magnetic field H_0, its rotating frequency Ω, the interface tension σ and the height $h(x,y)$ of the magnetic liquid layer. The wavenumber k of the interface mode is included in (3.1) to account for the magnetic boundary conditions $\lim_{z\to\pm\infty} \partial_z \phi = 0$ on the magnetic potential $\phi(x,y,z)$, which in the described case leads to $\phi^{(z\pm)}(x,y,z) = \phi(x,y)e^{\mp kz}$ (Rannacher & Engel 2007). Since we are only interested in stable solutions of the interface, one can assume that the time-dependent terms in (3.1) will only contribute with their mean values. This yields the Helmholtz-type differential equation for the interface

$$-\sigma_{eff}\nabla_\perp^2 h(x,y) + (\rho_0 - \rho_1)gh(x,y) = 0, \tag{3.2}$$

with $\nabla_\perp^2 = \partial_{xx} + \partial_{yy}$, where the influence of the rotating magnetic field is included in the wavenumber- and field-strength-dependent increased effective interface tension $\sigma_{eff} = (\mu_0 \chi^2 H_0^2)/(2(2+\chi)k) + \sigma$. Solving (3.2) in cylindrical geometry with respect to the boundary condition provided by the circular aluminium washer of diameter d

$$h\left(\frac{d}{2}, \varphi\right) = 0, \tag{3.3}$$

and the constant volume of both fluids

$$\int_0^{2\pi} \int_0^{d/2} h(r,\varphi)\, \mathrm{d}r\, \mathrm{d}\varphi = \text{const.}, \tag{3.4}$$
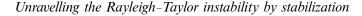
yields

$$h(r,\varphi) = A_1 \mathrm{J}_1(k_{eff}\, r) \cos(\varphi + \theta_1). \tag{3.5}$$

Here J_1 is a Bessel function of the first kind, $k_{eff} = \sqrt{|\rho_0 - \rho_1|g\sigma_{eff}^{-1}}$ and θ_1 determines the phase. The amplitude A_1 has been determined by fitting (3.5) to the reconstructed interface.

It is also worth mentioning that we observed a field-dependent rotational symmetric distortion of the surface, which was taken into account by adjusting the Bessel mode J_0 in addition, in order to describe the observed shape within the accuracy of the X-ray setup.

3.2. *Scaling of the pattern amplitude*

Figure 2(*b*) shows the outcome of the fitted pattern amplitude A_1 as a function of the control parameter $\varepsilon = 1 - H^2/H_c^2$ where H_c is the critical field strength for the perfect
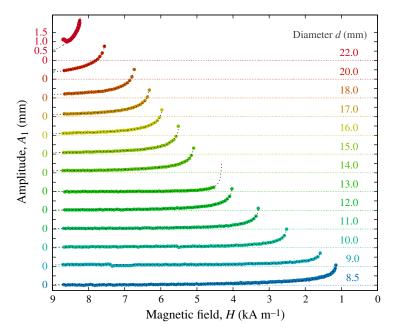
FIGURE 3. Dependence of the amplitude A_1 of the J_1-mode on the magnetic field strength H for different interface diameters d. The x axis is a mirror image to comply with the representation of the bifurcation.

bifurcation. However, before the pattern amplitude A_1 becomes unstable one observes a monotonic increase. The scaling of A_1 may be described by an amplitude equation. From symmetry considerations one expects an amplitude equation of the form

$$\tau_0 \dot{A}_1 = A_1 \varepsilon + \beta A_1^3 + b, \tag{3.6}$$

where b describes the imperfection at lowest order, as displayed in figure 2(*c*). By fitting the steady solution $A_1(\varepsilon)$ of the amplitude equation (3.6) to the recorded amplitude data it is possible to acquire the critical field strength H_c. The fitted stable branch of the imperfect subcritical pitchfork bifurcation in figure 2(*b*) shows remarkable agreement with the experimental data. One should note that it is not required to leave the stable branch of the bifurcation for this measurement. The critical field strength can therefore be determined without the actual occurrence of the RTI.

Figure 3 shows recorded amplitude datasets for different interface sizes. Each curve depicts a stable branch of the subcritical pitchfork bifurcation at the specific diameter. With decreasing diameter the field needed to stabilize the RTI decreases. At 8 mm (not shown) the interface tension alone is sufficient to suppress any growing mode. The magnitude of the imperfection b is varying between experiments. We suspect that the imperfection is caused by a remaining small tilt of the experimental setup, and/or inhomogeneities of the rotating magnetic field due to air bubbles in the experimental container. This imperfection is not a nuisance, but actually required for our measurement method of H_c. As soon as the slope of the measured amplitude starts to diverge, the measurement process is interrupted, because a further decrease of the magnetic field strength would lead to the onset of the RTI, causing the inconvenience of a new filling procedure.
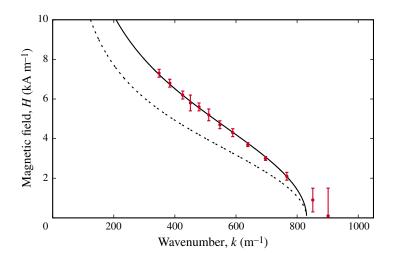
FIGURE 4. The critical field strength H_c of the RTI as a function of the wavenumber k of the unstable mode. The red data points show the measured values. The dashed line depicts the theoretical prediction for the stability boundary using the measured material parameters ρ_0, ρ_1, σ and the measured initial susceptibility $\chi_0 = 1.4$ of APG512a. The solid line shows the same but using a lowered effective susceptibility χ_{red}.

3.3. *The boundary of stability*

With the acquisition of the critical field strength H_c as a function of the interface diameter d, we measured the stability boundary $H_c(k)$ predicted by Rannacher & Engel (2007), as marked in figure 4 by red data points. The dashed line gives the stability boundary predicted by the model of Rannacher & Engel (2007) taking into account the measured densities and interfacial tension. In a first approach we select the measured initial susceptibility $\chi_0 = 1.4$ for a comparison with the model. The theoretical model by Rannacher & Engel (2007) was derived assuming a linear magnetization law $M(H) = \chi H$, with $\chi = $ const. However, as shown in figure 5(*a*), the magnetization of the ferrofluid APG512a is a nonlinear function of the internal magnetic field. The green data points display the values measured with a vibrating sample magnetometer (Lakeshore Inc., type 7404) versus the internal magnetic field (for details see Friedrich *et al.* 2012). The solid line stems from a fit of the data by the modified mean field model of second order (Ivanov & Kuznetsova 2001). Figure 5(*b*) displays the derivative of the magnetization curve, which has its maximum value $\chi_0 = 1.4$ at the origin and decays for higher values of the magnetic field. Since χ_0 is the highest value in the investigated field range [0 kA m^{-1}, 7 kA m^{-1}] the predicted stability boundary underestimates the measured values. The solid line in figure 4 is obtained by fitting a constant reduced magnetic susceptibility $\chi_{red} = 0.99$ to the data. According to figure 5(*b*), this value is well situated in the centre of the investigated interval.

It should be noted that a fit by an effective susceptibility is only a first approximation to cope with the nonlinear magnetization curve. An improved description would also have to deal with the fact that we use a finite, cylindrical container, which unavoidably generates an inhomogeneous magnetization. A combination of both intricacies would require a full numerical treatment.
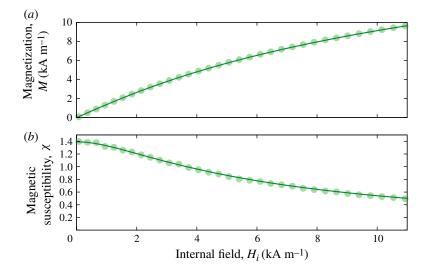
FIGURE 5. (*a*) Magnetization versus the internal magnetic field for the ferrofluid APG512a, where for clarity only every fifth data point is shown. The solid line displays a fit of the data by the modified mean field model of second order (Ivanov & Kuznetsova 2001). The tangential susceptibility $\chi_{ta} = \partial M/\partial H$ is displayed in (*b*).

Even though for wavenumbers larger than the capillary wavenumber $k_c = \sqrt{|\rho_0 - \rho_1|g/\sigma} = 831$ m^{-1} the system should be stable without the application of an external field, we observe (see figure 4) the occurrence of the instability at finite field strengths for the experiments corresponding to 851 and 902 m^{-1}. These two data points do not match the overall behaviour indicated by the theoretical prediction for an infinite geometry. In addition, their measurement errors, determined from fitting the recorded amplitude data by the static solution of (3.6), are in both cases comparatively large. For this reason, we consider them to be artifacts, caused by the imperfection – mainly the increasing influence of the forcing generated by the small circumference of the aluminium washer. Note, that a forcing term was not included in (3.1).

3.4. *Growth dynamics of the amplitude*

In addition to the static measurement, the procedure presented here can be used to record the dynamics of growth. This is utilized in an experiment with an interface diameter $d = 16$ mm. First we acquired the critical field strength by statically measuring the stable branch of the imperfect bifurcation. In this state we know the complete bifurcation diagram for the instability. After switching to the maximum applicable field strength (corresponding to ε_0), the control parameter is increased instantaneously to a supercritical value ε_1, as shown in figure 6(*a*). Now, the system is unstable and the J_1-mode will start to grow. By jumping back to a subcritical control parameter ε_2, the system can be forced back to a stable state, as long as the jump occurred early enough to reach a coordinate in the bifurcation diagram which is below the backward bifurcating unstable branch (cf. figure 6*b*). Figure 6(*c*) shows the temporal evolution of the amplitude A_1 of the J_1-mode at different waiting times in the supercritical state.
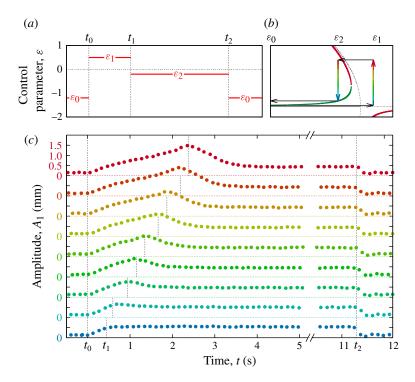
FIGURE 6. (*a*) Measurement protocol for the control parameter ε over time. (*b*) Bifurcation diagram with depicted dynamics of the experiment. Instantaneous jumps in the control parameter are shown as black arrows, amplitude growth is colour coded. (*c*) Dynamic measurement of the amplitude A_1 of the growing J_1-mode. Vertical grey dotted lines mark time points in the measurement protocol. The waiting time in the supercritical state is increased from bottom to top.

Since the critical field strength H_c and the bifurcation coefficients β and b were obtained by the static measurement, we can now use the acquired dynamic data to fit the dynamic amplitude equation. A phase-space representation of the previous plot can be seen in figure 7. The stable starting condition of the system is on the left-hand side. Since the minimum acquisition time of the X-ray detector is 134 ms we exclude points that are closer than one acquisition time to a jump in the control parameter. This restriction excludes all points gathered during the jump at t_2. Data recorded during amplitude increase (decrease) is colour coded in red (blue). Fitting the dynamic amplitude equation $\dot{A}_1(A_1)$ to the two data sets yields the characteristic time scale τ_0 of the first unstable mode of the RTI,

$$\tau_0 = (0.61 \pm 0.13) \text{ s}, \tag{3.7}$$

which shall be interpreted in relation to the capillary time

$$t_c = \left(\frac{\sigma}{g^3 |\rho_0 - \rho_1|} \right)^{1/4} = 66.4 \text{ ms.} \tag{3.8}$$
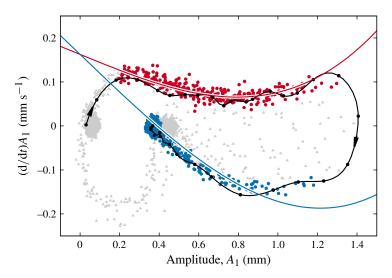
FIGURE 7. Phase space of the dynamic amplitude measurement (figure 6). Grey points mark the complete measured dataset. One sample recording is shown in black. The connecting line serves as a guide for the eye. Red and blue points mark selected data from rising or falling edges of the control parameter after t_0 and t_1 respectively as indicated in figure 6(*a*). The solid lines show the fitted dynamic amplitude equation.

4. Conclusions

In conclusion, we have experimentally proved the feasibility of a new stabilization mechanism for the RTI using magnetic fluids and azimuthally rotating magnetic fields. We were able further to show that the most unstable mode of the RTI is described by a subcritical pitchfork bifurcation of a Bessel mode. This allowed us to exploit the imperfection of the experimental setup to measure the critical field strength of the instability, without its actual occurrence. The stability boundary $H_c(k)$ was measured and compared with the prediction by Rannacher & Engel (2007). The model complies with our data within the parameter uncertainties when using a constant effective susceptibility, corresponding to its reduction at higher field strengths. Future work should refine this assumption by including the full nonlinear magnetization curve $M(H)$.

More importantly, a dynamic measurement method was proven to work that facilitates the suppression of an already unstable mode, and enabled us to force the growing mode back to its initial state. It was used to record the growth dynamics of the J_1-mode and acquire its characteristic time scale τ_0. Having precise control of the dynamics of the RTI renders this type of experiment a perfectly suited model system. In particular it now seems feasible to build a control loop to dynamically regulate the amplitude A_1, which would allow one to move along the unstable branch of the RTI.

Acknowledgements

References

EVANS, R., BENNETT, A. & PERT, G. 1982 Rayleigh–Taylor instabilities in laser-accelerated targets. *Phys. Rev. Lett.* **49** (22), 1639–1642.

FRIEDRICH, T., LANG, T., REHBERG, I. & RICHTER, R. 2012 Spherical sample holders to improve the susceptibility measurement of superparamagnetic materials. *Rev. Sci. Instrum.* **83** (4), 045106–045106.

GOLLWITZER, CH., MATTHIS, G., RICHTER, R., REHBERG, I. & TOBISKA, L. 2007 The surface topography of the Rosensweig instability – a quantitative comparison between experiment and numerical simulation. *J. Fluid Mech.* **571**, 455–474.

IVANOV, A. O. & KUZNETSOVA, O. B. 2001 Magnetic properties of dense ferrofluids: an influence of interparticle correlations. *Phys. Rev.* E **64** (4), 041405.

LEWIS, D. J. 1950 The instability of liquid surfaces when accelerated in a direction perpendicular to their planes. II. *Proc. R. Soc. Lond.* A **202**, 81–96.

RANNACHER, D. & ENGEL, A. 2007 Suppressing the Rayleigh–Taylor instability with a rotating magnetic field. *Phys. Rev.* E **75** (1), 016311.

RAYLEIGH, LORD 1883 Investigation of the character of the equilibrium of an incompressible heavy fluid of variable density. *Proc. Lond. Math. Soc.* **14**, 170–177.

RICHTER, R. & BLÄSING, J. 2001 Measuring surface deformations in magnetic fluid by radioscopy. *Rev. Sci. Instrum.* **72**, 1729–1733.

ROSENSWEIG, R. E. 1985 *Ferrohydrodynamics*. Cambridge University Press.

SMARR, L., WILSON, J., BARTON, R. & BOWERS, R. 1981 Rayleigh–Taylor overturn in super-nova core collapse. *Astrophys. J.* **246** (2), 515–525.

TAYLOR, SIR G. 1950 The instability of liquid surfaces when accelerated in a direction perpendicular to their planes. *Proc. R. Soc. Lond.* A **201** (1065), 192–196.

VÖLTZ, C., PESCH, W. & REHBERG, I. 2001 Rayleigh–Taylor instability in a sedimenting suspension. *Phys. Rev.* E **65**, 011404.

WOLF, G. 1969 Dynamic stabilization of Rayleigh–Taylor instability and corresponding dynamic equilibrium. *Z. Phys.* **227** (3), 291–300.

ZUIDEMA, H. & WATERS, G. 1941 Ring method for determination of interfacial tension. *Ind. Engng Chem. Anal. Edn* **13** (5), 312–313.